

Physiochemical, Mineralogical, Thermal and Kinetic Characterisation of Selected Coals from the Benue Trough and Anambra Basin, Nigeria

Bemgba B. Nyakuma^{a, b, *}, Segun A. Akinyemi^c, Syie L. Wong^d,
Olagoke Oladokun^e, Aliyu Jauro^f, and Tuan Amran T. Abdullah^b

^a Research Initiative for Sustainable Energy Technologies, North-Bank, Makurdi, Benue State, Nigeria

^b School of Chemical and Energy Engineering, Faculty of Engineering,
Universiti Teknologi Malaysia, Skudai, Johor, Malaysia

^c Department of Geology, Faculty of Science, Ekiti State University, Ado Ekiti, Ekiti State, Nigeria

^d Dpto. Matemática Aplicada, Ciencia Ingeniería Materiales Tecnología Electrónica,
Universidad Rey Juan Carlos, Madrid, Spain

^e Department of Chemical Engineering, Covenant University, Canaan Land, Ota, Ogun State, Nigeria

^f National Centre for Petroleum Research and Development, Abubakar Tafawa Balewa University, Bauchi State, Nigeria

*e-mail: bbnayax1@gmail.com

Received May 1, 2021; revised May 1, 2021; accepted July 15, 2021

Abstract—This study examined the physiochemical, mineralogical, thermal, and kinetic characteristics of selected Nigerian coals, namely; Chikila (CHK), Lafia Obi (LFB) and Okaba (OKB) from the Benue Trough and Anambra Basin. Physicochemical analyses revealed significant carbon, volatile matter, fixed carbon, and higher heating values (~25–30 MJ/kg) along with low contents of moisture and ash. The deduced properties indicate subbituminous to bituminous rank coals. The morphological, microstructure and elemental analyses revealed heterogeneous sized coal particles with a glassy lustre, which are ascribed to quartz, alumina, kaolinite, hematite, and other clay or aluminosilicate minerals. Thermal analysis under oxidative conditions indicated the coal samples are highly reactive, which resulted in significant degradation as evident in the high mass losses ($M_L = 91.59\text{--}94.04\%$) and low residual masses ($R_M = 5.96\text{--}8.41\%$), which occurred in the order LFB > OKB > CHK for M_L whereas R_M was CHK > OKB > LFB. Kinetic analysis values of activation energy (E_a) from 30.07 to 43.91 kJ/mol, frequency factor (A) from 1.16×10^{-02} to $6.73 \times 10^{-02} \text{ min}^{-1}$ and R^2 from 0.98–0.99 based on the Coats–Redfern model. The kinetic analysis indicated the coals are highly reactive and suitable for energy recovery.

Keywords: coal energy conversion, thermokinetics, Benue Trough basin, Nigeria

DOI: 10.3103/S1068364X21110065

1. INTRODUCTION

Coal is a high carbon content, brown-to-black coloured, organic sedimentary rock formed from the high temperature and pressure reactions on tectonically buried plant materials in the earth's crust [1, 2]. The formation of coal historically commenced about 290 million to 360 million years ago due to the physicochemical changes, which transformed vegetation into peat and eventually into the various ranks of coal. Hence, coal is a solid fossil-based fuel formed from the remnants of antediluvian plant life collected in peat bogs or coal forming swamps [3, 4]. Over the years, coal has become an integral part of the global energy mix due to its abundance and accessibility worldwide. Currently, coal accounts for 64% of globally economically recoverable fossil fuels (~1 trillion tonnes) when

compared to oil (19%) and natural gas [5]. The most significant deposits located in the United States, Russia, Australia, China, India, Indonesia, Germany, Poland and Ukraine collectively account for ~90% of the total global reserves [6]. However, energy data indicates that commercial coal mining is projected at 6.9 billion tonnes and occurs in over 50 countries worldwide [4].

In general, coal is utilised for the production of iron, steel, cement, chemicals, fuels, and fertilisers [7]. The primary utilisation of coal is for power generation, where it accounts for ~40% or about 8200 terawatt-hours (TWh) of electricity generated annually [8]. Coal-fired power generation provides cheap and reliable electricity required to provide the heat and power needs of domestic and industrial locations [8, 9]. Therefore, the utilisation of coal in developing coun-

tries is critical for infrastructural development, socio-economic growth, and poverty alleviation [10]. According to the IEA, coal-fired power generation could also address energy poverty [8], which currently affects 1.3–3.5 billion people or 50% of humanity who either have limited or zero access to electricity [11, 12]. The lack of electricity and related energy crises is prevalent in Africa's largest economy and most populous nation, Nigeria. Over the years, the country has experienced persistent low voltage, load shedding, intermittent power outages and extended blackouts [12, 13]. These challenges are ascribed to poor power generation and distribution along with dilapidated power infrastructure, which has caused transmission losses and system failures in the national electricity grid [14, 15].

According to energy analysts, the diversification of Nigeria's energy mix currently dominated by hydro-power and gas-fired electricity could address the current issues associated with power generation in Nigeria [16, 17]. Hence, the adoption of coal-fired electricity based on the vast coal reserves in Nigeria could serve as a practical panacea to the nation's energy crises [18, 19]. The nation's reserves of coal are estimated at 640 million proven and 2.75 billion tonnes of provisional tonnes, which are located across the six geopolitical regions of Nigeria [20, 21]. Despite the vast reserves, wide accessibility, and availability, the utilization of coal for electricity generation is non-existent in Nigeria [22, 23]. One of the widely reported reasons for zero coal utilisation is the lack of comprehensive data on the fuel and energetic properties of the various coal deposits in the country [18, 24]. The limited technical expertise and scientific knowledge along with the energy, economic, and environmental ramifications of coal utilisation also need to be addressed in detail. Therefore, this paper seeks to examine the physicochemical, mineralogical, thermal, and kinetic fuel properties of selected Nigerian coal samples from Chikila (CHK), Lafia Obi (LFB) and Okaba (OKB) in the Benue Trough and Anambra Basin.

2. EXPERIMENTAL

2.1. Materials and Sampling

The dark brown to black rock coal samples, namely; Chikila (CHK), Lafia Obi (LFB), and Okaba (OKB) were obtained from mines or seams located in the Benue Trough and Anambra Basin of Nigeria. Sampling was carried out by direct excavation from coal bed mines distributed across various locations in each seam to guarantee representative channel samples. The CHK coal was acquired from Chikila village in Guyuk town of Guyuk local government area (LGA) of Adamawa state, which is situated in the Upper Benue Trough of Nigeria. The LFB coal sample was acquired from Lafia-Obi LGA of Nasarawa state situated in the Middle Benue Trough of Nigeria. The OKB coal was acquired from Ankpa LGA in Kogi

State, which is located in the Anambra Basin. The rock sized coal samples were dry milled in a grinder (Panasonic Mixer MX-AC400, Malaysia) before sieving using the analytical sieve (Retsch™, Germany, Mesh size 60 or 250 μm) for further characterisation.

2.2. Methods

2.2.1. Physicochemical Analyses. The physicochemical analysis of the coal samples was examined by ultimate, proximate, and calorific analyses. The ultimate analysis deduced the carbon (C), hydrogen (H), nitrogen (N), and sulphur (S) composition using an elemental analyser (vario MACRO Cube, Germany), whereas the oxygen content was computed by difference from the sum of C, H, N and S. The proximate analysis was performed through thermogravimetric analysis (TGA) (Shimadzu TG-50, Japan) to determine moisture (M), volatile matter (VM), and ash (AC) compositions. The fixed carbon (FC) was then computed by difference from the sum of the M, VM, and AC. The calorific analysis was performed using a bomb calorimeter (IKA C2000, USA) based on ASTM standard D-2015 to determine the higher heating value (HHV).

2.2.2. Morphological and Microstructural Analyses. The morphologic and microstructure properties were determined by scanning electron microscopy (SEM) and energy dispersive X-ray (EDX) spectroscopy. SEM analysis was performed using the JEOL JSM IT 300 LV (Germany) analyser at the voltage of 20 kV and the working distance of 5 mm. For each test, the selected coal sample was spray deposited on carbon epoxy tape placed on grain mounts. Next, the sample was sputter-coated with gold (Au) using the thin film automatic sputter coater (Quorum Q150R S, UK) fitted with 57 mm diameter disc-style targets and operating at the pressure of 2×10^{-3} mbar. The samples were sputter-coated to avert the impacts of charging, damage to the electron beam, and increase the clarity of the images during the analysis. On completion, the grain mounts containing the samples were transferred to the SEM analyzer for morphology and microstructure analysis. The SEM micrographs were subsequently captured at a magnification of $\times 2000$. Lastly, EDX analyzer was performed on the analyser (JEOL JSM IT 300 LV, Germany) based on the point ID technique, which detects the elements present in the mapped zones of SEM micrographs. The average composition in weight per cent (wt %) of each element was determined by charge balance and computed by point ID using the software (AZTEC, Oxford Instruments, England).

2.2.3. Mineralogical Analysis. The mineral composition of the coal samples was examined by wavelength dispersive X-ray fluorescence (WDXRF) spectroscopy. The tests were performed using the WDXRF analyser (Rigaku, ZXS Primus II WDXRF, Japan),

which used rhodium (Rh) target end-window based X-ray tubes. The device is equipped with a smart sample loading system and a mapping feature for determining the topography and distribution of sample elements. Based on the pellet method, each sample was weighed, pelletized, and transferred to the WDXRF sample holder. The sample preparation process ensured the sensitivity, calibration, and reliability of the results. The sample test was then initiated for a run time of one minute after which the metal and non-metallic composition of each coal sample was computed by the WDXRF analyser. The oxides of each metal and non-metallic element for each coal sample were then computed after automatic corrections using the Rigaku XRF EZ-scan (Japan) software combined with the SQX fundamental parameters.

2.2.4. Thermal Analysis. The thermal properties were examined by thermogravimetric analysis (TGA) under oxidative and non-isothermal conditions using the TG Analyser (Shimadzu TG-50, Japan). During each TG run, 13 mg of each coal sample was weighed in an alumina crucible before ramping the furnace temperature from 27 to 1000°C based on the heating rate of 20°C/min under airflow at the rate of 20 mL/min. On completion, the TG furnace was cooled to ambient temperature using an automatic air blower. Next, the raw thermogram data were recovered for analysis using the Shimadzu Workstation (TA-60WS) thermal analysis software. The mass loss (TG, %) and derivative of mass loss (DTG, %/min) data were subsequently plotted against temperature (°C) in Microsoft Excel (2013). Next, the temperature profile characteristics (TPCs) of each coal sample was deduced based on the plots using the thermal analysis software. In the current study, the TPCs determined were the onset temperature (T_{ons}), midpoint temperature (T_{mid}), maximum peak decomposition temperature (T_{max}), offset temperature (T_{off}), mass loss (M_L , %) and residual mass (R_M , %). The TPCs provide critical insights into thermal degradation, potential decomposition yield, and product distribution during thermochemical conversion [25, 26].

2.2.5. Kinetic Analysis. The kinetic analysis was performed based on the integral graphical method of the Coats–Redfern Model (CRM). According to the model, the thermal decomposition of the coals under oxidative conditions can be represented as [27];

$$\frac{dx}{dt} = kf(x), \quad (1)$$

$$x = \frac{m_0 - m_t}{m_0 - m_f}. \quad (2)$$

The terms; $\frac{dx}{dt}$ represent the rate of reaction; k is the rate of reaction constant; $f(x)$ is the mechanism of the reaction model, and x is the ratio of the sample masses (m_0 is the initial; m_t is the fixed time; and m_f is

the final) thermally degraded during TGA. The reaction model term for n order of the reaction is given as;

$$f(x) = (1-x)^n. \quad (3)$$

Therefore, the decomposition rate and temperature dependence of the coal degradation process can be described by the Arrhenius equation given as;

$$k(T) = A \exp\left(-\frac{E_a}{RT}\right). \quad (4)$$

The term A denotes the frequency factor (min^{-1}); E_a is the reaction activation energy (kJ/mol); R is the molar gas constant (J/mol K); and lastly, T is the absolute temperature (K). When the oxidative thermal decomposition process occurs at a fixed heating rate,

the term $\beta = \frac{dT}{dt}$ is introduced and substituted into Eq. 1 to derive the relation;

$$\frac{dx}{dT} = \frac{A}{\beta} \exp\left(-\frac{E_a}{RT}\right) (1-x)^n. \quad (5)$$

After separation of variables, Eq. 4 can be rearranged to consider the decomposition of the coal at a fixed heating rate during TGA, which subsequently results in the relation;

$$\frac{dx}{(1-x)^n} = \frac{A}{\beta} \exp\left(-\frac{E_a}{RT}\right) dT. \quad (6)$$

Next, Eq. 6 can be integrated to derive the integral function for the reaction model that describes the thermal decomposition of the coal samples as given by the relation;

$$g(x) = \int_0^x \frac{dx}{(1-x)^n} = \frac{A}{\beta} \int_{T_0}^T \exp\left(-\frac{E_a}{RT}\right) dT \quad (7)$$

The term $g(x)$ in Eq. 7 represents the integral function of the reaction model that can be used to apply the Coats–Redfern model. Based on the approximate method of the CRM, Eq. 7 can be re-written as;

$$\ln\left[\frac{g(x)}{T^2}\right] = \ln\left[\frac{AR}{\beta E_a} \left(1 - \frac{2RT}{E_a}\right)\right] - \frac{E_a}{RT}. \quad (8)$$

The terms $\ln\left[\frac{AR}{\beta E_a} \left(1 - \frac{2RT}{E_a}\right)\right]$ in Eq. 8 can be reduced to $\ln\left[\frac{AR}{\beta E_a}\right]$ since $\left(1 - \frac{2RT}{E_a}\right)$ equate to unity. Hence, Eq. 8 becomes;

$$\ln\left[\frac{g(x)}{T^2}\right] = \ln\left[\frac{AR}{\beta E_a}\right] - \frac{E_a}{RT}. \quad (9)$$

In this study, the first-order reaction model was selected due to high sample conversion rates during TG analysis. Hence, Eq. 9 is modified as;

Table 1. Physicochemical fuel properties of selected nigerian coals

Coal Property	Symbol (Units)	Chikila (CHK)	Lafia Obi (LFB)	Okaba (OKB)
Carbon	C, wt %	73.55	61.22	61.40
Hydrogen	H, wt %	5.95	6.45	5.59
Nitrogen	N, wt %	1.67	1.13	1.44
Sulphur	S, wt %	0.57	1.54	0.66
Oxygen	O, wt %	18.26	29.65	30.92
Moisture	M, wt %	3.07	11.59	8.63
Volatile matter	VM, wt %	35.27	46.04	40.03
Ash	A, wt %	7.86	7.21	7.69
Fixed carbon	FC, wt %	53.80	35.16	43.65
Higher heating value	HHV, MJ/kg	30.83	26.05	24.86

$$\ln \left[\frac{-\ln(1-x)}{T^2} \right] = \ln \left[\frac{AR}{\beta E_a} \right] - \frac{E_a}{RT}. \quad (10)$$

The kinetic parameters E_a and A can be derived from the slope $-\frac{E_a}{R}$ and intercept $\ln \left[\frac{AR}{\beta E_a} \right]$ of the straight-line plots of $\ln \left[\frac{-\ln(1-x)}{T^2} \right]$ against $\frac{1}{T}$ which is based on the governing reaction mechanism of thermal degradation. The values of E_a and A describe the rate of the thermal reactions, which are dependent on the degree of conversion (x), temperature (T , K), and time (t , min) during the TG analysis.

3. RESULTS AND DISCUSSION

3.1. Physicochemical Properties

Table 1 shows the physicochemical properties of the selected Nigerian coals examined in this study. The results indicate that the coals contain high proportions of carbon ranging from 61.22% (LFB) to 73.55% (CHK) and oxygen from 18.26% (CHK) to 30.92% (OKB). As observed in Table 1, the higher heating value (HHV) occurred between 24.86 MJ/kg and 30.83 MJ/kg as observed for OKB and CHK coals, respectively. The highest HHV observed for CHK is explained by its high carbon but low oxygen and moisture contents. In comparison, the OKB coal has the highest oxygen contents among the samples, which implies it will exhibit higher thermal reactivity and oxidative degradation compared to LFB and CHK. However, LFB exhibited the highest moisture and volatile matter but low ash contents, which makes it the most suitable coal sample for gasification into syngas and fuel gases. Likewise, the thermal conversion of LFB could potentially yield higher volumes of condensable and non-condensable gases compared to CHK and OKB coals.

The rank classification of each coal was predicted according to the ASTM standard D388 [28]. Typically, the standard is employed to predict the rank, classification, and potential application of coal samples based on the HHV, particularly in the absence of petrographic and vitrinite analysis. According to the standard, coals with volatile matter above 31 wt % can be ranked or classified accordingly [3]. Based on the standard, CHK (HHV = 30.83 MJ/kg) is classified as high-volatile B bituminous coal with HHV values typically from 30.20 to 32.60 MJ/kg. The findings for CHK are in excellent agreement with several authors based on the vitrinite reflectance of $\%R_{\max} \approx 0.70$ in the literature [29, 30]. In contrast, LFB (HHV = 26.05 MJ/kg) is classified as high-volatile C bituminous and agglomerating coal with HHV values typically from 30.20 to 32.60 MJ/kg. However, Akinyemi et al. [31] reported that LFB coal is subbituminous based on its vitrinite reflectance of $\%R_{\max} \approx 0.39$, which contrasts markedly with [19, 29, 30, 32, 33] who have reported a similar classification (bituminous coal and $\%R_{\max} \approx 1.0$) as reported in this study. Lastly, OKB (HHV = 24.86 MJ/kg) is classified as Subbituminous A and non-agglomerating coal with HHV typically from 24.40 to 26.70 MJ/kg [3]. The subbituminous nature of OKB in this study is corroborated by the findings of Adeleke et al. [34] and Oboirien et al. [19] in the literature. Based on the above criteria, CHK and LFB are considered high-ranked coals, whereas OKB is considered low ranked coal. In addition to the potential applications earlier proposed, CHK and LFB could be also utilised for value-added applications such as the production of metallurgical coke, iron or steel. OKB could be utilised for producing thermal coal or for industrial thermal processes, power generation, or cement production.

3.2. Morphological and Microstructural Properties

The surface morphology and microstructure of the coal samples were examined by SEM spectroscopy. Figures 1–3 present the high-resolution SEM micrographs of CHK, LFB, and OKB coals examined at a magnification of $\times 2000$. The morphological and microstructural analysis using SEM presents valuable insights into the chemical composition, pore structure, orientation of particles, and surface composition of solid materials [35, 36]. It also provides an indication of the mineral components present in the structure of coals examined during the process [37]. The morphology of each coal is characterised by a rough, contoured, and compact (or sintered) surface with no evident macro- or micro-pores despite the heterogeneous sized and shaped particles randomly dispersed on the surfaces.

The coal particles observed in the SEM micrographs also exhibited a glassy sheen at the edges and contours, which indicates the presence of mineral or metallic constituents in their structure. The glassy or reflective nature of the surface particles observed on the coal surfaces could be due to the presence of aluminosilicate and iron-containing minerals such as quartz, kaolinite, calcite, and pyrite [38–40]. The mineralogical analysis of coals in previous studies have also detected gypsum, Jarosite, montmorillonite and compounds like sodium chlorate [30, 41, 42]. The metallic elements Ti, Mn, and Fe along with the minerals present in elemental and fused forms are also considered major determinants of surface morphology, thermochemical properties, and quality of the coal [43]. To examine this, the elemental composition of CHK, LFB, and OKB was examined by EDX spectroscopy as presented in the next section of the paper. Table 2 shows the micro-elemental composition of the CHK, LFB, and OKB examined by energy-dispersive X-ray (EDX) spectroscopy. The elements detected were; carbon, oxygen, aluminium, silicon, sulphur, calcium, and iron in various quantities.

As observed, a total of seven elements (namely; C, O, Al, Si, S, Ca, Fe) were detected in the CHK and LFB coals, although Ca was not detected (ND) in the OKB coal. In this study, the major elements defined as elements with weight per cent (wt %) above 1.00 wt % are carbon (C) and oxygen (O), whereas the minor (trace wt % < 1.00) elements detected were Al, Si, S, Ca, Fe, and Ca. The metallic elements detected in coal are typically associated with the presence of salts, clay or substituted porphines (or porphyrin rings) [3]. The metallic element Al indicates the presence of alumina (Al_2O_3); whereas Si is ascribed to quartz (SiO_2), which is considered the most abundant mineral on the earth's crust. The presence of Ca, Si, and O in combined form could indicate the presence of the calcium ino-silicate (or metasilicate) mineral (CaSiO_3) otherwise called Wollastonite, whereas Ca, C and O may be due to limestone (calcite) or gypsum ($\text{CaSO}_4 \cdot 2\text{H}_2\text{O}$).

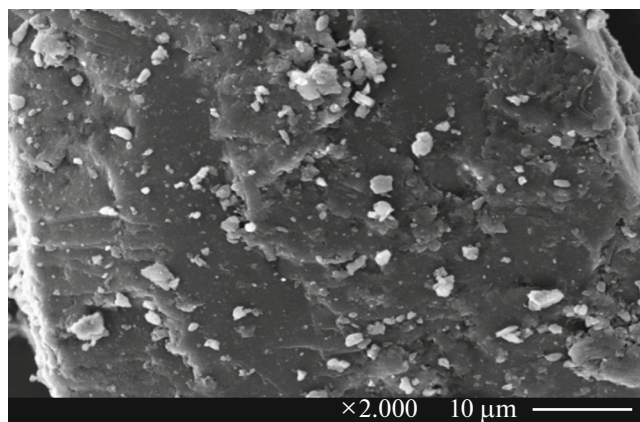


Fig. 1. HR-SEM images of Chikila Coal.

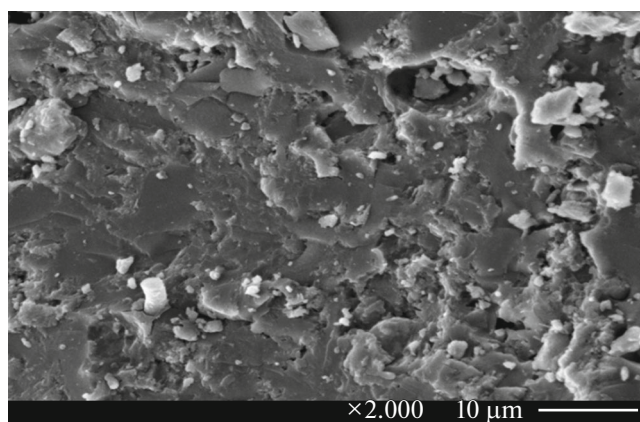


Fig. 2. HR-SEM images of Lafia-Obi Coal.

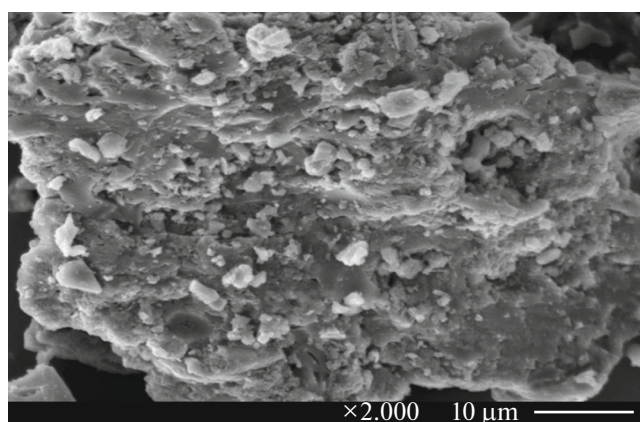


Fig. 3. HR-SEM images of Okaba (OKB) Coal.

The presence of limestone (termed coal balls) in coal beds is widely reported in the literature [44, 45]. The presence of Al and Si could also be ascribed to the clay (silicate) mineral kaolinite [$\text{Al}_2\text{Si}_2\text{O}_5(\text{OH})_4$]. The elements Fe and S indicate the presence of the sulphide

Table 2. EDX elemental composition of selected nigerian coals

Element	Symbol	Chikila Coal (CHK, wt %)	Lafia-Obi Coal (LFB, wt %)	Okaba Coal (OKB, wt %)
Carbon	C	86.37	79.83	76.04
Oxygen	O	12.81	19.24	21.77
Aluminium	Al	0.10	0.11	0.87
Silicon	Si	0.10	0.29	0.80
Sulphur	S	0.43	0.42	0.43
Calcium	Ca	0.09	0.05	ND
Iron	Fe	0.10	0.07	0.08

mineral pyrite in the coal structure. In general, EDX analyses revealed the CHK, LFB and OKB coals contain clay and metal-based minerals such as quartz, kaolinite, Wollastonite, gypsum, calcite, kaolinite, and other silicates, which denotes the high abundance of clay minerals in the coal samples examined in this study. Other studies have similarly detected the presence of these minerals in coal and coal fly [46, 47]. According to Barwood et al. [48], the accurate identification of clay minerals in coals is critical to utilisation during thermochemical conversion such as coal liquefaction. The findings of the study also indicated that the abundance of clay minerals presents crucial information on the environment of coal deposition. Furthermore, the chemical species found in coal are also considered an indication of chemical weathering [49, 50]. It also serves as a measure of the degree of coalification, rank, and the source of mineral matter in coal [43, 51, 52].

3.3. Mineralogical Properties

The mineralogical properties of CHK, LFB and OKB were examined by X-ray fluorescence (XRF) spectroscopy. Table 3 presents the computed mineralogical (metal oxides and non-metallic) compositions of each coal sample in this study. The XRF analysis revealed the presence of 23 major oxides and traces in the CHK and LFB coals, whereas a total of 30 were detected in OKB coal. The major oxides commonly detected in all the coal samples were; SiO₂, Al₂O₃, Fe₂O₃, CO₂, MgO, CaO, TiO₂, K₂O, Na₂O and SO₃ corresponding to the oxides of silicon, aluminium, iron, carbon, magnesium, calcium, titanium, potassium, sodium and sulphur. The highest composition of the oxides in the coal samples is due to silicon oxide (SiO₂) along with the alkali/alkali earth metal oxides (CaO, Al₂O₃, MgO, Na₂O, and K₂O). The presence of silicon oxide (SiO₂) and aluminium oxide (Al₂O₃) indicate the presence of quartz and alumina formed from the SiO₂-Al₂O₃ system [53, 54] along with kaolinite minerals in the structure of the coals [55, 56]. Furthermore, iron oxide (Fe₂O₃) may be due to the presence of hematite, which is one of the most

commonly detected minerals in soils and sedimentary rocks (such as shale and coal) formed from weathering processes. The oxide of titanium (TiO₂) detected in the coal samples may be largely due to ilmenite (manaccanite, FeTiO₃) and the naturally occurring minerals including rutile and anatase [57, 58]. According to Vassilev and Vassileva [59], TiO₂ could also originate from aragonite, brockite, calcite, iron sulphides, gypsum, mica, oxy-hydroxides and other organic or clay minerals. Lastly, the oxides of carbon (CO₂) and sulphur (SO₃) denote the organic nature or history of the coals.

In contrast, about 22 oxides of selected metals were detected in minor quantities in the coal samples. Most notably, the OKB coal contains the oxides Ga₂O₃, Y₂O₃, Rb₂O, Ar₂O₃, Nb₂O₅, BaO, La₂O₃, CeO₂, Nd₂O₃, Gd₂O₃, Er₂O₃, and WO₃, which were either detected in trace amounts in LFB or undetected in CHK. The findings indicate that OKB contains higher concentrations of oxides of alkaline earth (Ba), transition (Nb), rare earth (Ce, La, Nd, Gd, Er,) metals and the toxic oxides of the metalloid (Ar). The oxides of the rare earth elements (REE) indicate minerals of organic origins particularly apatite, calcite, feldspars, iron sulphides, mica, monazite, siderite, xenotime, and zircon [59]. The higher concentrations of the REE detected in the study also reveals the level of weathering, maturity, rank and classification of the coals. Based on the findings, the rank of the coals is in the order CHK > LFB > OKB, which is in good agreement with earlier submission based on ASMT D388. The concentrations of the REE and other elements in OKB conforms to its low-rank status compared to LFB and CHK, which suggests higher thermal reactivity or degradation during thermal conversion processes. Hence, the thermal degradation behaviour, decomposition pathways, and temperature profile characteristics of the coals were also examined in this study.

3.4. Thermal Properties

Figures 4 and 5 show the thermogravimetric (TG) and derivative (DTG) plots for the CHK, LFB, and

Table 3. XRF compositions of nigerian coals

Metal Oxide	Chikila Coal (CHK, wt %)	Lafia-Obi Coal (LFB, wt %)	Okaba Coal (OKB, wt %)
CO ₂	6.05	4.94	6.46
Na ₂ O	0.41	0.14	0.09
MgO	1.86	3.83	0.22
Al ₂ O ₃	20.61	10.88	27.41
SiO ₂	55.41	31.33	58.42
P ₂ O ₅	0.06	0.06	0.09
SO ₃	0.14	9.45	0.01
K ₂ O	1.23	0.23	0.30
CaO	1.48	14.41	1.32
TiO ₂	1.24	1.65	2.85
V ₂ O ₅	0.04	0.00	0.00
Cr ₂ O ₃	0.03	0.03	0.03
Fe ₂ O ₃	11.30	22.87	1.95
Co ₂ O ₃	0.01	0.04	0.04
NiO	0.02	0.04	0.06
CuO	0.02	0.03	0.02
ZnO	0.03	0.01	0.21
Ga ₂ O ₃	0.00	0.01	0.01
Ar ₂ O ₃	0.00	0.01	0.00
GeO ₂	0.02	0.00	0.00
Rb ₂ O	0.00	0.00	0.00
SrO	0.01	0.05	0.01
Y ₂ O ₃	0.00	0.01	0.03
ZrO ₂	0.01	0.01	0.02
Nb ₂ O ₅	0.00	0.00	0.00
BaO	0.00	0.00	0.08
La ₂ O ₃	0.00	0.00	0.06
CeO ₂	0.00	0.00	0.15
Nd ₂ O ₃	0.00	0.00	0.10
Gd ₂ O ₃	0.00	0.00	0.03
Er ₂ O ₃	0.00	0.00	0.01
WO ₃	0.00	0.00	0.01

OKB. The findings indicate that the oxidative and non-isothermal heating TGA process resulted in the rapid thermal degradation of the coal samples as evident in the downward Z shape curves, significant mass loss ($M_L > 90\%$) but low residual masses (R_M). The mass loss during TGA could be ascribed to the loss of volatile organic components or macerals in the structure of the coals. The organic components of coal are typically comprised of inertinite, vitrinite, and

liptinite groups [3]. Based on the rank, classification, and source of the coal the proportion of each organic components can range from 5–10% for liptinite, 50–90% for vitrinite, and 50–70% for inertinite. The thermochemical reactivity along with the yield and distribution of products from coal conversion is largely influenced by the proportion of macerals [60, 61], particularly vitrinite and inertinite fractions [62]. The loss of mass during coal degradation could also be

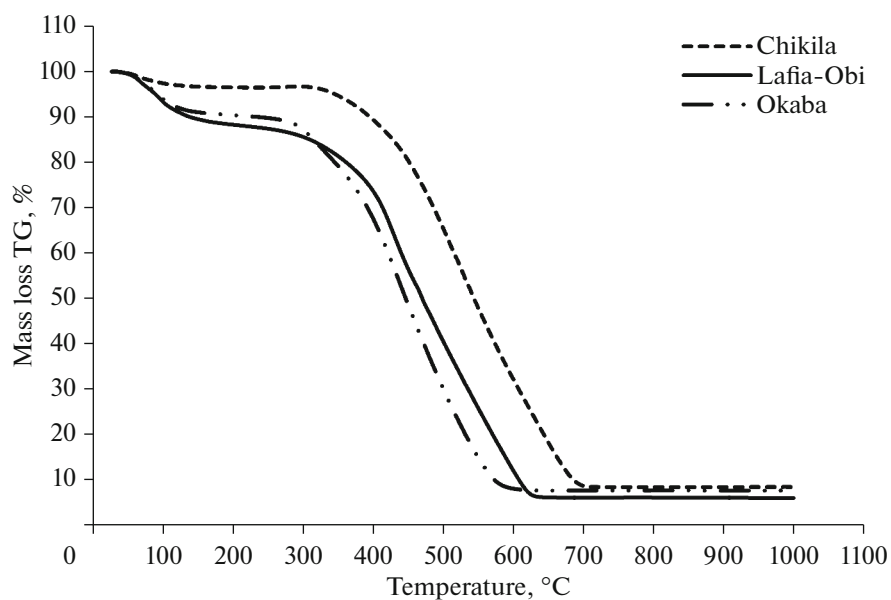


Fig. 4. TG plots for oxidative TG coal analysis.

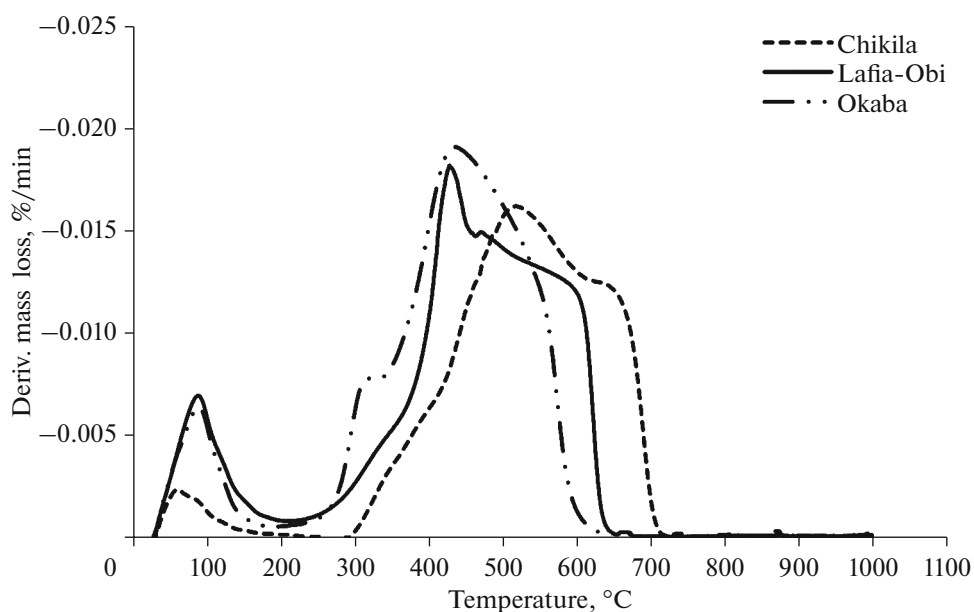


Fig. 5. DTG plots for oxidative TG coal analysis.

attributed to the degradation of lignocellulosic materials (resins, cellulose, lignin) originating from plants during the coalification process [63, 64].

The effect of the thermal degradation process on the mass loss (M_L), residual mass (R_M) and the corresponding temperature profile characteristics of the coals are presented in Table 4. The TPCs deduced in this study are; the onset (T_{ons}), midpoint (T_{mid}), and offset (T_{off}) temperatures. The results indicate that the mass loss (M_L , %) was in the range 91.59–94.04%,

whereas the residual mass (R_M , %) was from 5.96–8.41% for the coals. The M_L is in the order LFB > OKB > CHK, whereas the R_M is in the reverse order CHK > OKB > LFB. Based on the findings, LFB experienced the highest mass loss (M_L , %) along with the lowest residual mass (R_M , %), which indicates it is more thermally reactive when compared to OKB and CHK. In contrast, CHK was the least thermally reactive as it experienced the lowest mass loss (M_L , %) but the highest residual mass (R_M , %). The findings indi-

Table 4. Coal characteristic temperature and mass loss profiles

Coal sample	Code	Onset temp. (T_{ons} , °C)	Midpoint temp. (T_{mid} , °C)	Offset temp. (T_{off} , °C)	Mass loss (M_L , %)	Residual mass (R_M , %)
Chikila	CHK	394.94	530.54	657.27	91.59	8.41
Lafia-Obi	LFB	336.19	460.58	576.91	94.04	5.96
Okaba	OKB	321.70	436.77	548.58	92.35	7.65

Table 5. Characteristic coal TPCs for DTG plots and mass loss rates

Coal sample	Code	Dry peak temp. (T_{dry} , °C)	Drying rate, %/min	Devolatilization peak temp. (T_{dev} , °C)	Devolatilization rate, %/min
Chikila	CHK	60.40	1.04	517.61	7.17
Lafia-Obi	LFB	88.40	2.88	428.46	7.70
Okaba	OKB	89.51	2.62	436.14	7.89

cate that LFB and OKB are lower in rank compared to CHK due to their higher reactivity during TGA.

Typically, low ranked coals exhibit high thermal reactivity due to the presence of inert components and non-coking properties [65]. Furthermore, the structure of low ranked coals contains highly reactive functional groups, higher contents of H and O, along with higher pores and surface area compared to coals of higher ranks [66]. Hence, the higher contents of rare earth and alkali/alkali earth metals of LFB and OKB (as earlier surmised in Table 3) may account for the higher mass loss of the coals. The high reactivity of low-rank coals particularly at low temperatures can result in spontaneous combustion, thereby posing human safety and environmental risks during storage [66]. Hence, the TGA results also provide valuable insights into the health and safety of coal storage and utilization.

The TPCs also showed that thermal degradation revealed distinct values of onset (T_{ons}), midpoint (T_{mid}), and offset (T_{off}) temperatures for each coal examined. The analysis indicated that the onset (T_{ons}) ranged from 321.70 to 394.94°C, whereas the midpoint (T_{mid}), was from 436.77 to 530.54°C and the offset (T_{off}) was from 548.58 to 657.27°C. The findings indicate that the CHK exhibited the highest onset (T_{ons}), midpoint (T_{mid}), and offset (T_{off}) values of 394.94, 530.54, and 657.27°C, respectively, whereas the lowest values were observed for OKB. This observation confirms that CHK is more thermally stable compared to the lower-ranked OKB and LFB coals examined in this study. Further studies to examine the thermal reactivity of the coal samples through derivative thermal analysis (DTG).

The DTG against temperature plots for CHK, LFB, and OKB are presented in Fig. 5. The plots show several endothermic peaks of various sizes and shapes resulting from the thermal degradation process. The first set of small yet symmetric peaks can be observed

from RT to 200°C for all the coal samples. Based on the mass losses; CHK (3.483 wt %), LFB (11.732 wt %) and OKB (9.587 wt %) or $M_L < 12$ wt % during this stage, the thermal degradation could be ascribed to the loss of moisture and low molecular weight volatile coal components. The second stage is characterised by a larger set of asymmetric peaks compared to the first stage and was observed between 200 and 650°C for OKB and LFB whereas it was 700°C for CHK. The mass loss during this stage is due to the thermal degradation of macerals notably the inertinite and vitrinite fractions of the coals [62]. Based on the findings CHK requires a higher temperature range for thermal degradation compared to LFB and OKB, which further emphasises it is a higher-ranked coal. Table 5 presents the characteristic of coal TPCs for DTG plots and mass-loss rates.

The characteristic coal TPCs deduced from the DTG peaks showed that the maximum temperatures for drying occurred between 60.40°C (CHK) and 89.51°C (OKB), whereas the drying rates (%/min) were observed from 1.04 to 2.88%/min. The results further indicate the drying rate of LFB was the highest of the coals examined in this study, which could be ascribed to its high moisture content (11.59 wt %) compared to OKB and CHK. As earlier surmised, the second stage of the TGA process was characterised by a larger asymmetric peak culminating in a maximum value termed the devolatilization peak temperature (T_{dev} , °C). In this study, the T_{dev} was observed from 428.46°C (LFB) to the highest value of 517.61°C (CHK). The high T_{dev} is related to the effect of volatile matter (VM), which accounts for the thermal ignition and reactivity of carbonaceous materials [67]. As reported in Table 1, the volatile matter of CHK (35.27 wt %) is much lower than LFB (46.04 wt %), and OKB (40.03 wt %). Hence, the high T_{dev} value of CHK is explained by its comparatively lower VM, which accounts for its higher ignition temperature

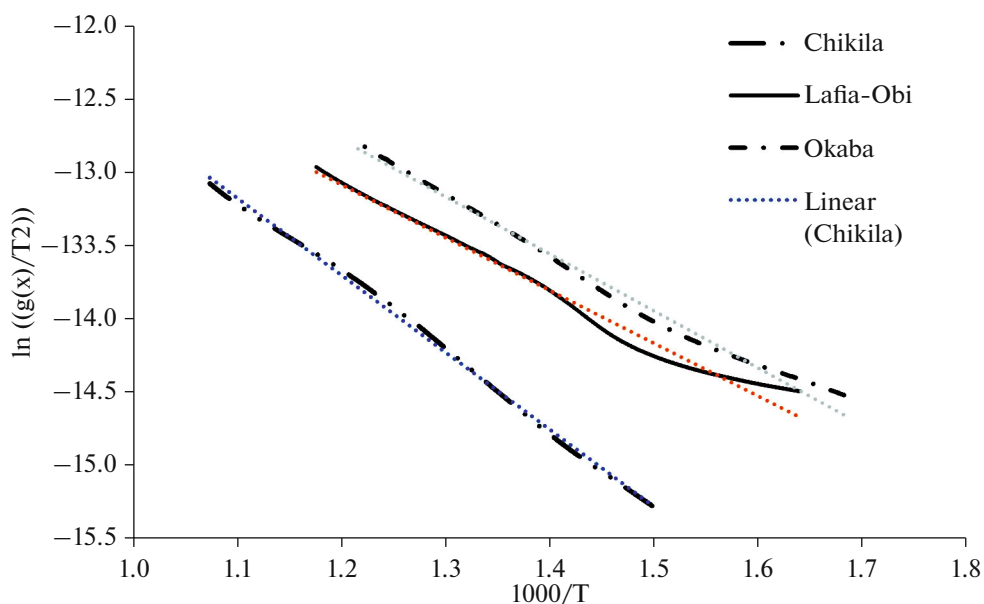


Fig. 6. CRM kinetic plots for thermal degradation of benue trough coals.

($T_{\text{ons}} = 394.94^{\circ}\text{C}$) reported in Table 4. Likewise, CHK has the lowest reactivity (due to its low VM and high ranked nature) as evident in its low devolatilization rate of 7.17%/min compared to 7.70%/min for LFB and 7.89%/min for OKB. The thermal reactivity of the coals can be further examined by kinetic analysis.

3.5. Kinetic Properties

The kinetic parameters; activation energy (E_a , kJ/mol) and frequency factor (A , min^{-1}) was computed based on the governing equations of the Coats–Redfern model. The E_a and A were calculated from the slope and intercept of the downward sloping kinetic plots in Fig. 6.

For the coal samples examined in this study, the value was computed as presented in Table 6. The E_a values range from 30.07 to 43.91 kJ/mol, whereas A is from $1.16 \times 10^{-02} \text{ min}^{-1}$ to $6.73 \times 10^{-02} \text{ min}^{-1}$ with the minima and maxima ascribed to LFB and CHK, respectively. The results indicate that the thermal degradation of the coals is highly reactive as evident in the low values of E_a and A in Table 6, which were computed at high R^2 values of 0.98–0.99. Furthermore,

the findings confirm that LFB is more thermally reactive when compared to the OKB and CHK in decreasing order. In comparison, Sonibare et al. [68] reported that the oxidative thermal analysis of selected coals from Nigeria are; E_a of 68.50 kJ/mol–90.90 kJ/mol, A of $4.3 \times 10^{01} \text{ min}^{-1}$ – $6.7 \times 10^{02} \text{ min}^{-1}$, and R^2 of 0.980–0.994. Hence, the values of CHK, LFB, and OKB in this study differ markedly from the findings from Sonibare et al. [68]. The differences could be ascribed to the variable physicochemical, macerals composition, rank classification, and reactivity of the coals.

4. CONCLUSIONS

The physiochemical, mineralogical, thermal and kinetic fuel properties of selected coal samples from the Benue Trough and Anambra Basins of Nigeria were examined in this study. The physicochemical characterisation revealed high compositions of carbon, volatile matter, fixed carbon but relatively low moisture, and ash. The calorific analysis revealed high heating values indicating mid-to-high ranked subbituminous and bituminous coals. The surface morphol-

Table 6. Calculated kinetic properties of coals based on Coats–Redfern model

Coal Sample	Code	Temperature range, $^{\circ}\text{C}$	Regression Coefficient (R^2)	E_a , kJ/mol	A , min^{-1}
Chikila	CHK	394.94–657.27	0.998	43.91	6.73×10^{-02}
Lafia-Obi	LFB	336.19–576.91	0.988	30.07	1.16×10^{-02}
Okaba	OKB	321.70–548.58	0.996	32.48	2.41×10^{-02}

ogy and microstructure revealed randomly dispersed coal particles with a glassy sheen, heterogeneous sizes, and shapes, as observed in the SEM/EDX analyses. Based on the mineralogical analysis, the oxides of silicon, aluminium, iron, carbon, magnesium, calcium, titanium, potassium, sodium and sulphur were detected in major quantities along with minor quantities of 22 other metals and non-metal elements. The findings indicate the presence of alkali/alkali earth metal oxides along with aluminosilicate and clay minerals such as quartz, alumina, kaolinite, and hematite. The thermal analysis examined under oxidative environment revealed high mass loss ($M_L = 91.59\text{--}94.04\%$) but low mass of residuals ($R_M = 5.96\text{--}8.41\%$) for each sample. The high thermal degradation behaviour and mass-loss rates could be ascribed to devolatilization and maceral decomposition of the coals. Kinetic analysis showed that the selected coal samples are highly reactive as evident in the low values of E_a and A computed at high R^2 values of $0.98\text{--}0.99$ using the Coats–Redfern model. Overall, the findings indicate that the selected coal samples have a high potential for energy recovery by oxidative conversion technologies such as pulverised coal combustion.

ACKNOWLEDGMENTS

The authors wish to acknowledge the Hydrogen Fuel Cell at Universiti Teknologi Malaysia (UTM) for the TGA runs. Many thanks also accrue to Universiti Malaysia Pahang (UMP) for the technical assistance with the XRF. The surface analysis (SEM/EDX) section of the University Industrial Research Laboratory (UiRL, UTM) is also gratefully acknowledged.

CONFLICT OF INTEREST

The authors declare that they have no conflicts of interest.

REFERENCES

- Speight, J.G., *Coal-Fired Power Generation Handbook*, Hoboken, NJ: Wiley, 2013, vol. 1.
- Gräbner, M., *Industrial Coal Gasification Technologies Covering Baseline and High-Ash Coal*, Chichester: Wiley, 2014.
- Speight, J.G., *The Chemistry and Technology of Coal*, Boca Raton, FL: CRC Press, 2012, 3rd ed.
- Basic coal facts, in *Coal Factsheet, 2017*, London: World Coal Assoc., 2017.
- The Global Value of Coal*, Paris: Int. Energy Agency, 2012, 1st ed.
- Countries with the biggest coal reserves, *Min. Technol. Mag.*, 2020, Jan. 6.
- Miller, B.G., *Clean Coal Engineering Technology*, Oxford: Butterworth-Heinemann, 2016, vol. 2.
- Global coal demand by forecast for 2000–2024, in *Analysis and Forecasts to 2024*, Paris: Int. Energy Agency, 2020.
- IEA-OECD, *Energy Indicators*, 2002, vol. 1, pp. 1–30.
- IEA-CCC, Cambodia: Two coal power plants built in Preah Sihanouk, in *Coal Power Projects*, London: IEA Clean Coal Centre, 2020.
- Nerini, F.F., Broad, O., Mentis, D., Welsch, M., Bazilian, M., and Howells, M., *Energy*, 2016, vol. 95, pp. 255–265.
- Adewuyi, O.B., Lotfy, M.E., Akinloye, B.O., Howlander, H.O.R., Senjyu, T., and Narayanan, K., *Appl. Energy*, 2019, vol. 245, pp. 16–30.
- Emodi, N.V., The energy sector in Nigeria, in *Energy Policies for Sustainable Development Strategies: The Case of Nigeria*, Singapore: Springer, 2016, pp. 9–67.
- Emodi, N.V. and Yusuf, S.D., *Int. J. Energy Econ. Policy*, 2015, vol. 5, pp. 335–351.
- Emovon, I., Samuel, O.D., Mgbemena, C.O., and Adeyeri, M.K., *Int. J. Integr. Eng.*, 2018, vol. 10, no. 1.
- Mohammed, Y., Mustafa, M., Bashir, N., and Mokhtar, A., *Renewable Sustainable Energy Rev.*, 2013, vol. 22, pp. 257–268.
- Oyedepo, S.O., *Renewable Sustainable Energy Rev.*, 2014, vol. 34, pp. 255–272.
- Ohimain, E.I., *Int. J. Energy Power Eng.*, 2014, vol. 3, pp. 28–37.
- Oboirien, B., North, B.C., Obayopo, S., Odusote, J., and Sadiku, E., *Energy Strategy Rev.*, 2018, vol. 20, pp. 64–70.
- Obaje, N.G., *Geology and Mineral Resources of Nigeria*, Berlin: Springer-Verlag, 2009, vol. 120.
- Chukwu, M., Folayan, C., Pam, G., and Obada, D., *J. Combust.*, 2016, vol. 2016, pp.
- Nyakuma, B., Jauro, A., Oladokun, O., Bello, A., Alkali, H., Modibo, M., and Abba, M., *Petrol. Coal*, 2018, vol. 60, pp. 641–649.
- Nyakuma, B.B. and Jauro, A., *GeoScience Eng.*, 2016, vol. 62, pp. 6–11.
- Nyakuma, B.B. and Jauro, A., *GeoScience Eng.*, 2016, vol. 62, pp. 1–5.
- Nyakuma, B., Oladokun, O., Abdullah, T., Ojoko, E., Abdullahi, M., El-Nafaty, A., and Ahmed, A., *Coke Chem.*, 2018, vol. 61, pp. 424–432.
- Nyakuma, B., Oladokun, O., Akinyemi, S., Ojoko, E., Jacob, G., Abdullah, T., Alkali, H., and Al-Shatri, A., *Coke Chem.*, 2019, vol. 62, pp. 371–378.
- Coats, A.W. and Redfern, J.P., *Nature*, 1964, vol. 201, pp. 68–69.
- ASTM D388-12: Standard Classification of Coals by Rank*, West Conshohocken, PA: ASTM Int., 2012.
- Jauro, A., Chigozie, A., and Nasirudeen, M., *Sci. World J.*, 2008, vol. 3, pp. 79–81.
- Akinyemi, S.A., Nyakuma, B.B., Jauro, A., Adebayo, O.F., Olaolorun, O.A., Adegoke, A.K., Aturamu, A.O., Adetunji, A., Gitari, W.M., and Mudzielwana, R., *Energy Geosci.*, 2020, vol. pp. 1–7.
- Akinyemi, S.A., Adebayo, O.F., Nyakuma, B.B., Adegoke, A.K., Aturamu, O.A., Olaolorun, O.A., Adetun-

- ji, A., Hower, J.C., Hood, M.M., and Jauro, A., *Int. J. Coal Sci. Technol.*, 2020, vol. 7, pp. 26–42.
32. Adeyinka, J.S. and Akinbode, F., *Indian J. Eng. Mater. Sci.*, 2002, vol. 9, no. 3, pp. 177–180.
 33. Amoo, L.M., *Fuel*, 2015, vol. 140, pp. 178–191.
 34. Adeleke, A., Onumanyi, P., and Ibitoye, S., *Petrol. Coal*, 2011, vol. 53, pp. 1–8.
 35. *JEOL-JSM IT 300 LV SEM Microscope: Brochure*, Freising: JEOL, 2017.
 36. Sengupta, P., Saikia, P.C., and Borthakur, P.C., *J. Sci. Res.*, 2008, vol. 67, pp. 812–818.
 37. Nyakuma, B.B., *Coke Chem.*, 2019, vol. 62, pp. 394–401.
 38. Akinyemi, S., Gitari, W., Akinlua, A., and Petrik, L., Mineralogy and geochemistry of sub-bituminous coal and its combustion products from Mpumalanga Province, South Africa, in *Analytical Chemistry*, London: InTechOpen, 2012, ch. 2.
 39. Querol, X., Fernández-Turiel, J., and López-Soler, A., *Fuel*, 1995, vol. 74, pp. 331–343.
 40. Liu, G., Vassilev, S.V., Gao, L., Zheng, L., and Peng, Z., *Energy Convers. Manage.*, 2005, vol. 46, pp. 2001–2009.
 41. Vassileva, C.G. and Vassilev, S.V., *Fuel Process. Technol.*, 2006, vol. 87, pp. 1095–1116.
 42. Silva, L.F., Ward, C.R., Hower, J.C., Izquierdo, M., Waanders, F., Oliveira, M.L., Li, Z., Hatch, R.S., and Querol, X., *Coal Combust. Gasif. Prod.*, 2010, vol. 2, pp. 51–65.
 43. Xu, Y., Liang, H., and Zhang, N., *Energy Explor. Exploit.*, 2019, vol. 37, pp. 1162–1181.
 44. Scott, A. and Rex, G., *Philos. Trans. R. Soc., B*, 1985, vol. 311, pp. 123–137.
 45. DeMaris, P.J., *J. Geol. Soc.*, 2000, vol. 157, pp. 221–228.
 46. Luo, Y., Ma, S., Zhao, Z., Wang, Z., Zheng, S., and Wang, X., *Ceram. Int.*, 2017, vol. 43, pp. 1–11.
 47. Ibarra, J., Palacios, J., and de Andrés, A.M., *Fuel*, 1989, vol. 68, pp. 861–867.
 48. Barwood, H.L., Curtis, C.W., Guin, J.A., and Tarrer, A.R., *Fuel*, 1982, vol. 61, pp. 463–469.
 49. Akinyemi, S.A., Gitari, W.M., Petrik, L.F., Nyakuma, B.B., Hower, J.C., Ward, C.R., Oliveira, M.L.S., and Silva, L.F.O., *Sci. Total Environ.*, 2019, vol. 663, pp. 177–188.
 50. Akinyemi, S.A., Gitari, W.M., Thobakgale, R., Petrik, L.F., Nyakuma, B.B., Hower, J.C., Ward, C.R., Oliveira, M.L.S., and Silva, L.F.O., *Environ. Geochem. Health*, 2020, vol. 42, pp. 2771–2788.
 51. Vassilev, S.V., Kitano, K., and Vassileva, C.G., *Fuel*, 1996, vol. 75, pp. 1537–1542.
 52. Dai, S., Li, T., Jiang, Y., Ward, C.R., Hower, J.C., Sun, J., Liu, J., Song, H., Wei, J., and Li, Q., *Int. J. Coal Geol.*, 2015, vol. 137, pp. 92–110.
 53. Vassilev, S.V. and Vassileva, C.G., *Fuel Process. Technol.*, 1996, vol. 47, pp. 261–280.
 54. Dai, S., Zhao, L., Peng, S., Chou, C.-L., Wang, X., Zhang, Y., Li, D., and Sun, Y., *Int. J. Coal Geol.*, 2010, vol. 81, pp. 320–332.
 55. Liu, X., Yan, Z., Wang, H., and Luo, Y., *J. Nat. Gas Chem.*, 2003, vol. 12, pp. 63–70.
 56. Dill, H., Kus, J., Dohrmann, R., and Tsoy, Y., *Int. J. Coal Geol.*, 2008, vol. 75, pp. 225–240.
 57. Zhang, W., Zhu, Z., and Cheng, C.Y., *Hydrometallurgy*, 2011, vol. 108, pp. 177–188.
 58. Filippou, D. and Hudon, G., *JOM*, 2009, vol. 61, p. 36.
 59. Vassilev, S.V. and Vassileva, C.G., *Fuel Process. Technol.*, 1997, vol. 51, pp. 19–45.
 60. Landais, P., Muller, J.-F., Michels, R., Oudin, J.-L., and Zaugg, P., *Fuel*, 1989, vol. 68, pp. 1616–1619.
 61. Košina, M. and Heppner, P., *Fuel*, 1984, vol. 63, pp. 838–846.
 62. Zhao, Y., Hu, H., Jin, L., He, X., and Wu, B., *Fuel Process. Technol.*, 2011, vol. 92, pp. 780–786.
 63. Xie, W., Stanger, R., Lucas, J., Wall, T., and Mahoney, M., *Fuel*, 2013, vol. 103, pp. 1023–1031.
 64. Sun, Q.-L., Li, W., Chen, H.-K., and Li, B.-Q., *J. China Univ. Min. Technol.*, 2003, vol. 32, pp. 664–669.
 65. de Lourdes Ilha Gomes, M., Osório, E., and Faria Vilela, A.C., *Mater. Res.*, 2006, vol. 9, pp. 91–95.
 66. Kim, J., Lee, Y., Ryu, C., Park, H.Y., and Lim, H., *Korean J. Chem. Eng.*, 2015, vol. 32, pp. 1297–1304.
 67. Basu, P., *Biomass Gasification and Pyrolysis: Practical Design and Theory*, Burlington, MA: Academic 2010.
 68. Sonibare, O., Ehinola, O., Egashira, R., and KeanGiap, L., *J. Appl. Sci.*, 2005, vol. 5, pp. 104–107.